Rapid Communications

Magnetic dichroism in the Kondo insulator SmB_6

W. T. Fuhrman,[1,2,*] J. C. Leiner,[3,4,5] J. W. Freeland,[6,†] M. van Veenendaal,[7,6] S. M. Koohpayeh,[2] W. Adam Phelan,[2,8] T. M. McQueen,[2,8,9] and C. Broholm[2,9,10]

[1]*Center for Nanophysics and Advanced Materials, Department of Physics, University of Maryland, College Park, Maryland 20742, USA*
[2]*Institute for Quantum Matter and Department of Physics and Astronomy, The Johns Hopkins University, Baltimore, Maryland 21218, USA*
[3]*Center for Correlated Electron Systems, Institute for Basic Science (IBS), Seoul 08826, Korea*
[4]*Department of Physics and Astronomy, Seoul National University, Seoul 08826, Korea*
[5]*Neutron Scattering Division, Oak Ridge National Laboratory, Oak Ridge, Tennessee 37831, USA*
[6]*Advanced Photon Source, Argonne National Laboratory, Argonne, Illinois 60439, USA*
[7]*Department of Physics, Northern Illinois University, DeKalb, Illinois 60115, USA*
[8]*Department of Chemistry, The Johns Hopkins University, Baltimore, Maryland 21218, USA*
[9]*Department of Materials Science and Engineering, The Johns Hopkins University, Baltimore, Maryland 21218, USA*
[10]*NIST Center for Neutron Research, Gaithersburg, Maryland 20899, USA*

(Received 15 April 2018; published 9 January 2019)

Samarium hexaboride (SmB_6) is a purported topological Kondo insulator, with theory predicting that the experimentally observed metallic surface states manifest from a topologically nontrivial insulating bulk band structure. The insulating bulk itself is driven by strong correlations, and both bulk and surface are known to host compelling magnetic and electronic phenomena. We employed x-ray absorption spectroscopy and x-ray magnetic circular dichroism at the Sm $M_{4,5}$ edges to probe the surface and bulk magnetic properties of Sm^{2+} and Sm^{3+} within SmB_6. We observed an unexpected antialignment to the applied field of the Sm^{3+} magnetic dipole moment below $T = 75$ K and of the total orbital moment of samarium below 30 K. The total bulk magnetization at 2 K is, however, positive and driven by Sm^{2+} Van Vleck susceptibility as well as 1% paramagnetic impurities with $\mu_{\text{eff}} = 5.2(1)\mu_B$. This indicates the diamagneticlike Sm^{3+} magnetism is only a portion of the net magnetization, partially offsetting the response of paramagnetic impurities known within the bulk.

DOI: 10.1103/PhysRevB.99.020401

The growing interest and application of topology in condensed matter physics has renewed investigations into SmB_6, a cornerstone material of condensed matter and materials science which has now been studied for more than 50 years [1–3]. Evidence continues to grow in support of the claim that SmB_6 is a topological Kondo insulator, with an insulating bulk at low temperatures and a topologically protected metallic surface, though there is not universal agreement [3–9].

In light of the potential topological aspects of SmB_6, great attention has been focused on its surface phenomena [7,10–13]. The strongly correlated nature of the insulating state implies that topological surface states should also be strongly correlated, with potentially exotic implications [14–16]. Complicating and enriching matters, magnetic impurities are common in SmB_6, introducing in-gap states and disrupting the surface state [17–20]. Samarium vacancies, which are difficult to avoid in floating-zone grown crystals, also produce states in the gap and may contribute to low-temperature properties such as thermal transport [21,22].

Recently, there have been a variety of unexpected experimental observations surrounding the low-energy magnetism in SmB_6 (e.g., quantum oscillations, optical conductivity, specific heat), with debate persisting over the origin of these measurements (surface/bulk and intrinsic/extrinsic) [18,23–28]. Understanding the magnetism of SmB_6 is of crucial importance because the protection of surface states relies on the preservation of time reversal symmetry [29]. Here, we report the surface- and bulk-sensitive x-ray magnetic circular dichroism (XMCD) measurements which directly probe the magnetizable components of Sm^{3+} and Sm^{2+}, thus offering a unique view into the low-energy magnetism in SmB_6. We measure vacuum-cleaved and nominally pure, stoichiometric SmB_6 as well as vacuum-cleaved Sm-deficient and carbon-doped samples. Surprisingly, the data reveal the net magnetic moment carried by Sm^{3+} is antialigned to the applied field for temperature (T) below 75 K despite positive bulk magnetization. This component is readily observed at the surface via electronic yield XMCD and indicated at similar magnitude by bulk-sensitive fluorescence yield XMCD. We relate this observation to known paramagnetic impurities within these samples and infer that Sm^{3+} is antiferromagnetically coupled with larger moment paramagnetic impurities.

SmB_6 crystals in nominally stoichiometric, carbon-doped, and $Sm_{1-x}B_6$ versions were grown using the floating-zone (FZ) technique as described by Phelan *et al.* [31]. Starting materials were polycrystalline SmB_6 rods (Testbourne Ltd., 99.9%). Previous elemental analysis indicated rare-earth and Alkaline-earth metal impurities at the 10^3 ppm scale present in starting materials and grown samples. These impurities form stable hexaborides with similar lattice parameters to

*wfuhrman@schmidtsciencefellows.org
†freeland@anl.gov

SmB_6 and thus readily occupy the Sm site. Summing up their concentrations indicates approximately 2% (1% magnetic with weighted average moment $\mu_{avg} = 5\mu_B$) impurities per formula unit. Extensive details about the concentrations and ubiquity of impurities in samples grown from these starting materials can be found in the Supplemental Material of Ref. [19].

The x-ray absorption spectroscopy (XAS) and XMCD measurements were conducted at beamline 4-ID-C of the Advanced Photon Source located at Argonne National Laboratory. SmB_6 crystals were notched to facilitate (100) cleavage. Crystals were cleaved after placement in the vacuum chamber (8×10^{-9} Torr) for measurement. Surface- and bulk-sensitive XAS and XMCD spectra were collected simultaneously using total electron yield (TEY) and total fluorescence yield (TFY), respectively, with circularly polarized x rays in a near normal (80°) configuration. The applied field was along the beam direction and it defines the positive $\hat{z}$ direction. The TEY mode probes approximately the first 2 nm of the SmB_6 surface, while TFY is bulk sensitive. The XMCD spectra were obtained point by point by subtracting right from left circular polarized XAS data. Measurements were taken for both positive and negative applied field directions and then we take a difference of these two spectra $\text{XMCD} = \frac{1}{2}[\text{XMCD}(H_z > 0) - \text{XMCD}(H_z < 0)]$ to eliminate polarization-dependent systematic errors. The correct sign of the XMCD spectrum was confirmed in a subsequent measurement against a known paramagnetic response. The stoichiometric sample central to this study was cleaved more than 24 h before measurement, sufficient time for complete surface reconstruction [32].

The isotropic and dichroic x-ray absorption spectra were calculated using XCLAIM [30] in the atomic limit [33,34], which is appropriate for the largely localized rare-earth $4f$ electrons. The Hamiltonian includes a spin-orbit interaction in the $3d$ and $4f$ orbitals and Coulomb interactions in the $4f$ shell and between the $4f$ shell and the $3d$ core hole. Parameters were obtained in the Hartree-Fock limit and the values for the Coulomb interaction were scaled down to 80% to account for screening effects. The calculated spectra are consistent with pure, divalent, and trivalent Sm compounds. Fits of the relative contributions of Sm^{2+} and Sm^{3+} allow for a small shift in energy (<1 eV) with fixed relative energy profiles.

The XAS near the M_5 (1080 eV) and M_4 (1105 eV) absorption edges [Fig. 1(a)] show distinct peaks from $Sm^{2+}(4f^6)$ and $Sm^{3+}(4f^5)$ in both the TEY and TFY channels. At the M edges, the bulk-sensitive TFY XMCD signal is weak and distorted by self-absorption effects, and so we proceed first with an analysis of the surface-sensitive TEY XMCD [35–37]. In a field at low temperatures, the presence of both divalent and trivalent Sm is clearly visible in the pre-edge region of M_5 where their dichroism features are opposite. Additionally, the main line of Sm^{2+} causes a significant negative dichroic feature around 1077 eV that is not present in the dichroic spectrum of Sm^{3+}. This dichroic spectrum is evidence of magnetizable moments at the surface of SmB_6. Because this response is observed in vacuum-cleaved samples, it cannot be attributed to the formation of surface oxides. Subtle changes in the dichroic features do occur following exposure to air, however, the fundamental

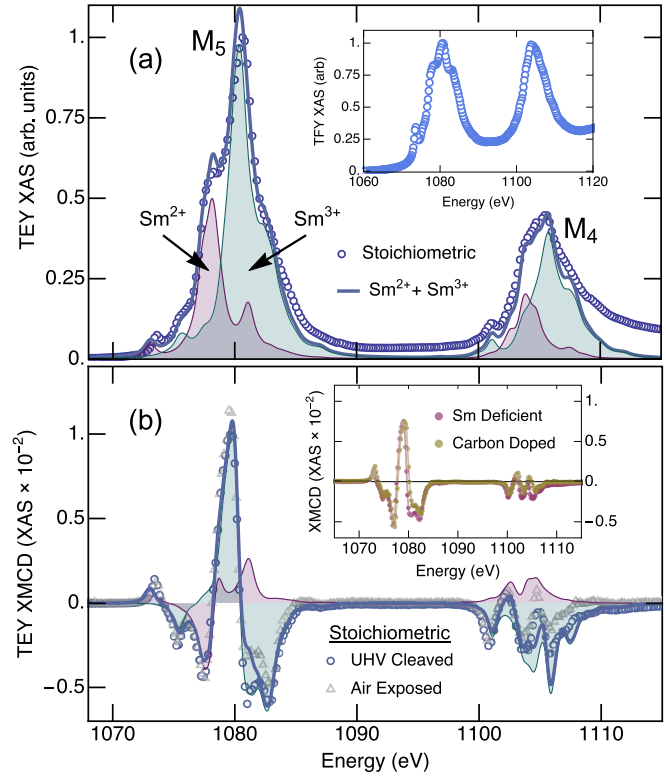

FIG. 1. XAS and XMCD spectra at $T = 8$ K, $\mu_0 H = 5$ T. Data were normalized by scaling the maximum at the M_5 edge (1079 eV). Shaded portions show relative contributions of Sm^{2+} and Sm^{3+}. (a) TEY shows the XAS of the surface (approximately 2 nm thickness), while TFY spectra show the bulk response (inset). (b) XMCD TEY and linear combination of Sm^{2+} and Sm^{3+} XMCD spectra calculated with XCLAIM [30]. XMCD was similar for a sample exposed to air (gray triangles). The inset shows XMCD of Sm-deficient and carbon-doped samples.

conclusion remains unaltered as the qualitative behavior of Sm^{2+} and Sm^{3+} is unchanged (i.e., Sm^{3+} orientation relative to the field does not change). The TEY XMCD in the field is similar for carbon-doped, and Sm-deficient samples [inset of Fig. 1(b)], with integrated mean-squared XMCD ($\int_{M_{4,5}} \sqrt{\text{XMCD}^2}$) of 0.017 (pure), 0.014 (Sm deficient), 0.013 (carbon doped). This indicates that the conditions of the initial sample that yield dichroic features are robust against other common impurities/defects. We thus infer that impurities known to be present at the 2% level are the predominant extrinsic factor relating to magnetizable Sm^{3+} moments.

At higher temperatures, the TEY XMCD is dominated by Sm^{2+} [Fig. 2(a)]. This contribution is evidenced by the Sm^{2+} pre-edge M_5 peak at 1073.5 eV which shows little temperature dependence. While the Van Vleck type $J = 0$ Sm^{2+} paramagnetism has only weak temperature dependence, free $J = 5/2$ Sm^{3+} carries a magnetic moment which should give rise to a Curie term $\propto 1/T$ in the corresponding magnetic susceptibility. Indeed, upon cooling below 75 K, a substantial feature at M_5 develops along with a weaker M_4 structure. However, the Sm^{3+} leading edge of M_4 (1100.5 eV) and fitted Sm^{3+} contribution show these dichroic features are associated

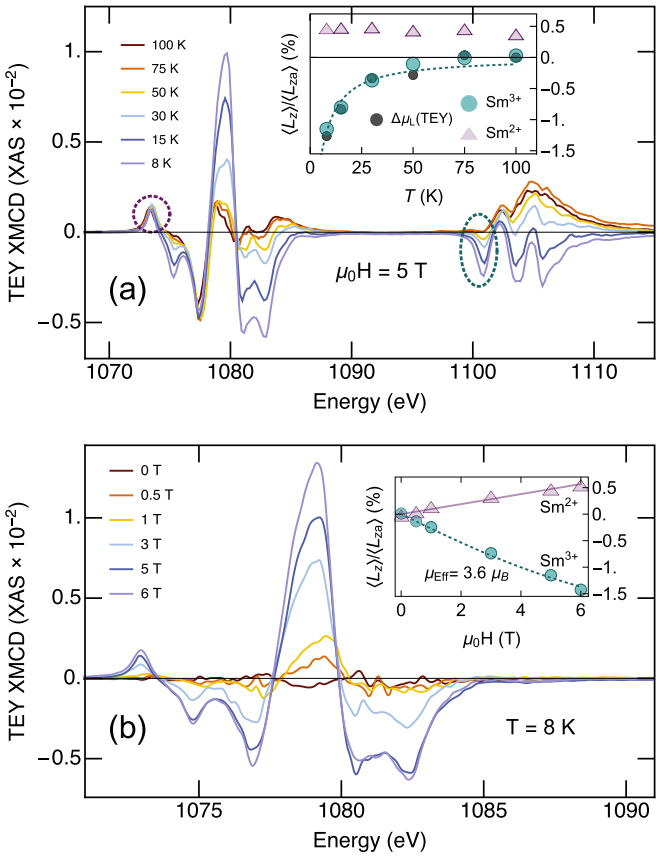

FIG. 2. TFY (surface) XMCD temperature and magnetic field dependence. (a) XMCD temperature dependence. Circled energies in the main panel indicate TEY XMCD spectra indicative of a single valence (1073.5 eV for Sm^{2+} and 1100.5 eV for Sm^{3+}). The inset shows the temperature dependence of the fitted Sm^{2+} and Sm^{3+} XMCD amplitudes and integrated ΔXMCD relative to 100 K ($\propto\Delta\mu_L$). (b) Magnetic field response of the M_5 edge TEY XMCD at 8 K. The inset shows the contributions from Sm^{2+} and Sm^{3+}. In the insets, the dotted lines show a Langevin fit [$\mu_{eff} = 3.6(9)\mu_B$, concentration 2.7(5)%] of the combined temperature dependence below 75 K and field dependence at 8 K.

with magnetized Sm^{3+} which is antialigned with the field rather than simply free paramagnetic moments.

In addition to the fitting described above, a sum rule analysis directly provides the Sm orbital moment through integration of the XMCD spectra over both the M_4 and M_5 edges [Fig. 2(a) inset] [38]. Given the weak temperature dependence of the Van Vleck Sm^{2+} component, the total orbital moment extracted from the TEY XMCD through a sum rule analysis is expected to follow the fitted Sm^{3+} component, offset by a constant. At high temperatures, the total orbital moment is positive, changing sign as the temperature is reduced below 30 K. This change in sign to a negative total orbital moment at low temperatures is model-independent evidence of a net negative orbital magnetic moment carried by Sm at low T. Subtracting off the high-T (100-K) Sm^{2+} component, we can compare the change in orbital moment (related to Sm^{3+}) to the expected Hund's rule value of $\langle L_{z_a}\rangle = 5$, finding $\Delta\langle L_z\rangle/\langle L_{z_a}\rangle = 1.5\%$ of the total Sm as magnetized Sm^{3+} at 8 K and 6 T. For reference, at 8 K and 6 T, small-moment Sm^{3+} ($\mu_{eff} = 0.85\mu_B$) yields 14% of its saturated moment while large-moment impurities ($\mu_{eff} \approx 5$) should be magnetized to 63% of their saturated moment.

The temperature and field dependence of the change in TEY (surface) XMCD, $\Delta\langle L_z\rangle/\langle L_z a\rangle$, can be fit by a negative Langevin function, $L(x) = c(\coth(x) - 1/x)$, where c is the concentration and x is the product of effective moment, field, and inverse temperature, $x = \mu_{eff}\,\mu_o H/(k_B T)$. This fit yields $\mu_{eff} = 3.6(9)\mu_B$ with a concentration of 2.7(5)% of the total population of Sm at saturation. This moment is larger than the Sm^{3+} moment, but close to the weighted average impurity moment. The implied concentration is also similar to the impurity concentration. In zero field [Fig. 2(b)], the TEY XMCD shows no evidence of magnetization beyond the experimental detection limit (<2% of the 5-T response at the M_5 peak, 1079.5 eV), an indication against surface ferromagnetism at 8 K. However, these magnetic components may have a magnetically ordered phase at sufficiently low temperatures, as suggested by hysteretic magnetotransport [39].

The bulk-sensitive TFY XMCD also indicates dichroic features within the bulk of SmB_6 [Fig. 3(b)]. If the bulk XMCD signal were entirely Sm^{2+} in origin, it would be expected to carry the weak temperature dependence seen of Sm^{2+} in TEY. However, upon cooling, the trailing edge of M_5 develops a dichroic feature which mirrors that of the surface (1081–1083 eV). The TEY and TFY dichroic features are similar in magnitude, and the change in integrated TFY XMCD decreases with lowering temperature. This is indicative of negative-moment magnetizable Sm^{3+} within the bulk as well as at the surface of SmB_6.

To contextualize the dichroic features associated with Sm^{3+} with the net magnetic properties of bulk SmB_6, we investigated the magnetization and susceptibility of the stoichiometric sample [Fig. 3(a)], reported previously without analysis [31]. A flattening of the susceptibility [Fig. 3(a) inset] occurs at 60 K, forming a broad hump before an eventual upturn at low T. The rounded maximum suggests short-range antiferromagnetic correlations. The low-T upturn is variable across samples of SmB_6 and can be attributed to a Curie-like susceptibility of weakly interacting magnetic impurities. At low temperatures, $M(H)$ is well fit by the sum of a linear component ($M = 0.0052\mu_B T^{-1}$ f.u.$^{-1}$) associated with Van Vleck magnetism and a Langevin function of 1% magnetic impurities with an effective moment $5.2(1)\mu_B$ [Fig. 3(a)]. Such fits have been shown to be effective over wide ranges of impurity concentrations, fields, and temperatures in SmB_6 [18]. The overall positive moment seen in bulk magnetization measurements indicates the predominant contribution to the low-T uniform magnetization is not the negative-moment Sm^{3+} magnetism seen by XMCD. However, Sm^{3+} coupled antiferromagnetically to larger moment impurities would appear antialigned with the field when observed independently.

The observed bulk magnetization is also consistent with the screening of magnetic impurities known to be in these samples from a previous elemental analysis [19]. While the XAS edges probed here limit sensitivity to Sm $4f$ electrons, previously described moment screening in Gd-doped SmB_6 provides a basis for comparison [18]. Assuming a similar effect, the expected moment screening of the bulk magnetization for 1% magnetic impurities (known to be present through elemental

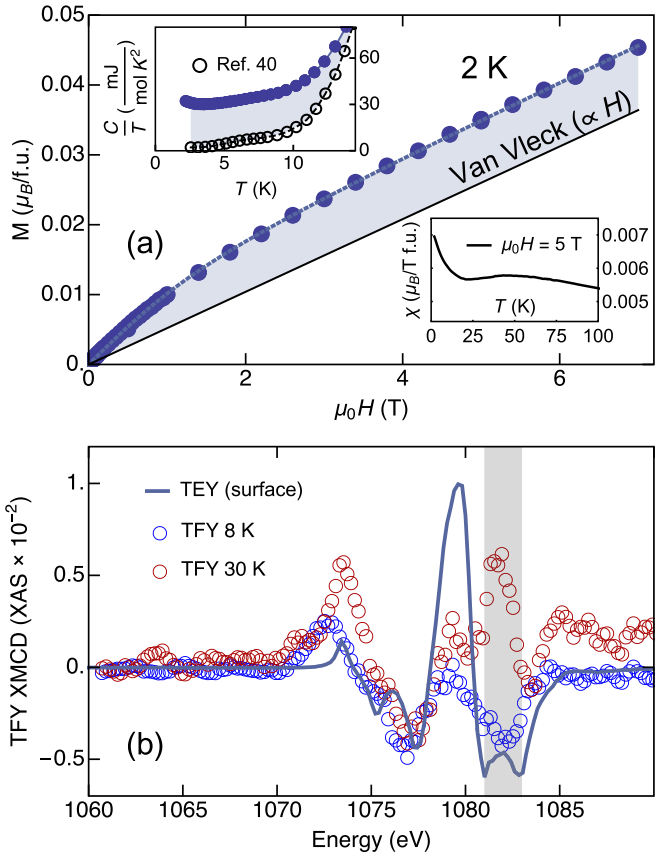

FIG. 3. Bulk properties of nominally pure SmB_6 sample. (a) The magnetization data are fit by a Van Vleck contribution (solid black line) and a paramagnetic impurity contribution (shaded) of 1% impurites with $\mu_{\text{eff}} = 5.2\mu_B$. Insets show the susceptibility taken at 5 T and heat capacity with a comparison to the previously published heat capacity of a high-purity sample [40]. We attribute shaded portions to impurities. Sample data also appear in the Supplemental Material of Ref. [19], without fitting. (b) TFY XMCD (bulk). At 8 K, a negative dichroic feature develops from 1081 to 1083 eV as for TEY. The temperature dependence counterindicates solely Sm^{2+}.

analysis [19]) would be 10% ($0.05\mu_B$), similar to the inferred bulk Sm^{3+} of order 1% of $\mu_{Sm} = 0.85\mu_B$ Sm^{3+} ($0.0085\mu_B$). The enhanced low-temperature heat capacity seen in our stoichiometric sample relative to a high-purity sample [Fig. 3(a) inset] is also consistent with the enhanced heat capacity associated with impurities and moment screening. High-quality starting materials yield SmB_6 samples with more than an order of magnitude smaller heat capacity at 2 K [40].

Polishing has a more substantial effect than carbon doping and Sm vacancies on Sm valence in our samples. Our stoichiometric, *in situ* vacuum-cleaved samples have a TEY valence at 8 K of 2.65(3) while previously measured polished samples grown from the same starting materials are dominated by Sm^{3+} [31]. Temperature dependence of the valence of the stoichiometric-cleaved sample shows a weak minimum at approximately 20 K, consistent with previous reports [41,42]. Importantly, all cleaved samples clearly show a dichroic response from Sm^{2+}, a distinct component of the intrinsic magnetism of SmB_6 and an indication that the intermediate valence phase is being probed. This, as well as the close proximity to a trivial insulating phase dictated by valence, indicates that caution is warranted in preparing and analyzing materials for which topological properties are measured [6].

We have observed a dichroic response for magnetizable Sm^{3+} below 75 K in SmB_6 via XMCD. The net magnetizable moment is antialigned with the applied field and paramagneticlike. The XMCD signal is insensitive to carbon doping and Sm deficiencies, indicating the negative Sm^{3+} moment is robust in the presence of other potential defects and impurities. By comparison to the net positive magnetization, we relate this Sm^{3+} to shared impurities, well known to be at the level of 2% (1% magnetic) in the samples measured [19]. The role of the boron framework is unknown, though there are previous indications of the importance of phonon coupling in the low-energy regime, and recent reports indicate that there is substantial overlap of the samarium and boron electron wave functions [43].

The positive bulk magnetization distinctly requires that the observed negative Sm^{3+} moment is not the predominant magnetization within the bulk. Nonetheless, the bulk-sensitive TFY XMCD, though complicated by self-absorption effects, indicates a negative Sm^{3+} moment. If the observed XMCD is intrinsic and present within the bulk, this implies the Kondo singlet ground state is modified by the magnetic field despite previous magnetization measurements on higher-purity samples showing almost exclusively Van Vleck magnetization to at least 60 T [44]. An exotic form of diamagnetism has been proposed at very low fields for SmB_6 [45]. However, given the impact of even modest impurity concentrations on the low-energy physics within SmB_6 (and present in our samples in appreciable quantities), a natural explanation for our observations is that the magnetizable Sm^{3+} antialigns to the applied field as a consequence of strong coupling to larger moment paramagnetic impurities. In this way the diamagneticlike response that we detect for Sm^{3+} can be associated with bulk compensated paramagnetism.

We note that XMCD of another floating-zone sample with a small magnetic impurity concentration (inferred by magnetization) was recently reported [46]. The total moment of Sm^{3+} was reported as aligned with the field at the surface (TEY), with a very small contribution antialigned within the bulk (TFY). In contrast, we observe an antialigned moment for Sm^{3+} at the surface and within the bulk occurring at similar magnitudes. Both results are consistent with our interpretation of magnetic impurities dramatically altering the magnetic behavior of Sm^{3+} within the bulk and surface of SmB_6.

This project was supported by UT-Battelle LDRD 3211-2440. The work at IQM was supported by the U.S. Department of Energy, Office of Basic Energy Sciences, Division of Material Sciences and Engineering under Grant No. DE-FG02-08ER46544. W.T.F. is grateful to the ARCS foundation and the Schmidt Science Fellows program, in partnership with the Rhodes Trust, for the partial support of this work. M.v.V. was supported by the U.S. Department of Energy (DOE), Office of Basic Energy Sciences, Division of Materials Sciences and Engineering under Award No. DE-FG02-03ER46097. Work at Argonne National Laboratory was supported by the U. S. DOE, Office of Science, Office of Basic Energy Sciences, under Contract No. DE-AC02-06CH11357.

[1] H. A. Eick and P. W. Gilles, J. Am. Chem. Soc. **81**, 5030 (1959).
[2] T. Kasuya, K. Takegahara, T. Fujita, T. Tanaka, and E. Bannai, J. Phys., Colloq. **40**, C5 (1979).
[3] S. Wolgast, Ç. Kurdak, K. Sun, J. W. Allen, D.-J. Kim, and Z. Fisk, Phys. Rev. B **88**, 180405(R) (2013).
[4] M. Dzero, K. Sun, V. Galitski, and P. Coleman, Phys. Rev. Lett. **104**, 106408 (2010).
[5] F. Lu, J. Z. Zhao, H. Weng, Z. Fang, and X. Dai, Phys. Rev. Lett. **110**, 096401 (2013).
[6] V. Alexandrov, M. Dzero, and P. Coleman, Phys. Rev. Lett. **111**, 226403 (2013).
[7] D. Kim, S. Thomas, T. Grant, J. Botimer, Z. Fisk, and J. Xia, Sci. Rep. **3**, 3150 (2013).
[8] Y. S. Eo, A. Rakoski, J. Lucien, D. Mihaliov, C. Kurdak, P. F. S. Rosa, D.-J. Kim, and Z. Fisk, arXiv:1803.00959.
[9] P. Hlawenka, K. Siemensmeyer, E. Weschke, A. Varykhalov, J. Sánchez-Barriga, N. Shitsevalova, A. Dukhnenko, V. Filipov, S. Gabáni, K. Flachbart *et al.*, Nat. Commun. **9**, 517 (2018).
[10] A. Stern, M. Dzero, V. Galitski, Z. Fisk, and J. Xia, Nat. Mater. **16**, 708 (2017).
[11] V. Alexandrov, P. Coleman, and O. Erten, Phys. Rev. Lett. **114**, 177202 (2015).
[12] X. Zhang, N. P. Butch, P. Syers, S. Ziemak, R. L. Greene, and J. Paglione, Phys. Rev. X **3**, 011011 (2013).
[13] J. Jiang, S. Li, T. Zhang, Z. Sun, F. Chen, Z. Ye, M. Xu, Q. Ge, S. Tan, X. Niu *et al.*, Nat. Commun. **4**, 3010 (2013).
[14] P. Nikolić, Phys. Rev. B **90**, 235107 (2014).
[15] K. Akintola, A. Pal, S. Dunsiger, A. Fang, M. Potma, S. Saha, X. Wang, J. Paglione, and J. Sonier, npj Quantum Mater. **3**, 36 (2018).
[16] W. Fuhrman, J. Leiner, P. Nikolić, G. E. Granroth, M. B. Stone, M. D. Lumsden, L. DeBeer-Schmitt, P. A. Alekseev, J.-M. Mignot, S. Koohpayeh *et al.*, Phys. Rev. Lett. **114**, 036401 (2015).
[17] D.-J. Kim, J. Xia, and Z. Fisk, Nat. Mater. **13**, 466 (2014).
[18] W. T. Fuhrman, J. R. Chamorro, P. A. Alekseev, J.-M. Mignot, T. Keller, P. Nikolic, T. M. McQueen, and C. L. Broholm, Nat. Commun. **9**, 1539 (2018).
[19] W. Phelan, S. Koohpayeh, P. Cottingham, J. Tutmaher, J. Leiner, M. Lumsden, C. Lavelle, X. Wang, C. Hoffmann, M. Siegler *et al.*, Sci. Rep. **6**, 20860 (2016).
[20] W. Fuhrman and P. Nikolić, arXiv:1807.00005.
[21] M. E. Valentine, S. Koohpayeh, W. A. Phelan, T. M. McQueen, P. F. S. Rosa, Z. Fisk, and N. Drichko, Phys. Rev. B **94**, 075102 (2016).
[22] M. Boulanger, F. Laliberté, M. Dion, S. Badoux, N. Doiron-Leyraud, W. Phelan, S. Koohpayeh, W. Fuhrman, J. Chamorro, T. McQueen *et al.*, Phys. Rev. B **97**, 245141 (2018).
[23] N. J. Laurita, C. M. Morris, S. M. Koohpayeh, P. F. S. Rosa, W. A. Phelan, Z. Fisk, T. M. McQueen, and N. P. Armitage, Phys. Rev. B **94**, 165154 (2016).
[24] P. K. Biswas, Z. Salman, T. Neupert, E. Morenzoni, E. Pomjakushina, F. von Rohr, K. Conder, G. Balakrishnan, M. C. Hatnean, M. R. Lees, D. M. Paul, A. Schilling, C. Baines, H. Luetkens, R. Khasanov, and A. Amato, Phys. Rev. B **89**, 161107 (2014).
[25] Z. Xiang, B. Lawson, T. Asaba, C. Tinsman, L. Chen, C. Shang, X. H. Chen, and L. Li, Phys. Rev. X **7**, 031054 (2017).
[26] M. Hartstein, W. Toews, Y.-T. Hsu, B. Zeng, X. Chen, M. C. Hatnean, Q. Zhang, S. Nakamura, A. Padgett, G. Rodway-Gant *et al.*, Nat. Phys. **14**, 166 (2018).
[27] H. Shen and L. Fu, Phys. Rev. Lett. **121**, 026403 (2018).
[28] N. Harrison, Phys. Rev. Lett. **121**, 026602 (2018).
[29] L. Fu, C. L. Kane, and E. J. Mele, Phys. Rev. Lett. **98**, 106803 (2007).
[30] J. Fernández-Rodríguez, B. Toby, and M. van Veenendaal, J. Electron Spectrosc. Relat. Phenom. **202**, 81 (2015).
[31] W. A. Phelan, S. M. Koohpayeh, P. Cottingham, J. W. Freeland, J. C. Leiner, C. L. Broholm, and T. M. McQueen, Phys. Rev. X **4**, 031012 (2014).
[32] V. Zabolotnyy, K. Fürsich, R. Green, P. Lutz, K. Treiber, C.-H. Min, A. Dukhnenko, N. Shitsevalova, V. Filipov, B. Kang *et al.*, Phys. Rev. B **97**, 205416 (2018).
[33] B. T. Thole, G. van der Laan, J. C. Fuggle, G. A. Sawatzky, R. C. Karnatak, and J.-M. Esteva, Phys. Rev. B **32**, 5107 (1985).
[34] J. B. Goedkoop, B. T. Thole, G. van der Laan, G. A. Sawatzky, F. M. F. de Groot, and J. C. Fuggle, Phys. Rev. B **37**, 2086 (1988).
[35] M. Pompa, A. M. Flank, P. Lagarde, J. C. Rife, I. Stekhin, M. Nakazawa, H. Ogasawara, and A. Kotani, Phys. Rev. B **56**, 2267 (1997).
[36] M. Nakazawa, H. Ogasawara, A. Kotani, and P. Lagarde, J. Phys. Soc. Jpn. **67**, 323 (1998).
[37] G. van der Laan and A. I. Figueroa, Coord. Chem. Rev. **277**, 95 (2014).
[38] P. Carra, B. T. Thole, M. Altarelli, and X. Wang, Phys. Rev. Lett. **70**, 694 (1993).
[39] S. Wolgast, Y. S. Eo, T. Öztürk, G. Li, Z. Xiang, C. Tinsman, T. Asaba, B. Lawson, F. Yu, J. W. Allen, K. Sun, L. Li, Ç. Kurdak, D.-J. Kim, and Z. Fisk, Phys. Rev. B **92**, 115110 (2015).
[40] M. Orendáč, S. Gabáni, G. Pristáš, E. Gažo, P. Diko, P. Farkašovský, A. Levchenko, N. Shitsevalova, and K. Flachbart, Phys. Rev. B **96**, 115101 (2017).
[41] M. Mizumaki, S. Tsutsui, and F. Iga, J. Phys.: Conf. Ser. **176**, 012034 (2009).
[42] Y. Utsumi, D. Kasinathan, K.-T. Ko, S. Agrestini, M. Haverkort, S. Wirth, Y. Wu, K. Tsuei, D. Kim, Z. Fisk *et al.*, Phys. Rev. B **96**, 155130 (2017).
[43] P. J. Robinson, X. Zhang, T. McQueen, K. H. Bowen, and A. N. Alexandrova, J. Phys. Chem. A **121**, 1849 (2017).
[44] B. Tan, Y.-T. Hsu, B. Zeng, M. C. Hatnean, N. Harrison, Z. Zhu, M. Hartstein, M. Kiourlappou, A. Srivastava, M. Johannes *et al.*, Science **349**, 287 (2015).
[45] O. Erten, P.-Y. Chang, P. Coleman, and A. M. Tsvelik, Phys. Rev. Lett. **119**, 057603 (2017).
[46] K. Chen, T.-C. Weng, G. Schmerber, V. N. Gurin, J.-P. Kappler, Q. Kong, F. Baudelet, A. Polian, and L. Nataf, Phys. Rev. B **97**, 235153 (2018).